Solid-State and Nanoparticle Synthesis of EuSxSe1-x Solid-Solutions

Haydee A. Dalafu, Nicholas Rosa, Derak James, Dane Asuigui, Michael McNamara, Akira Kawashima, Shun Omagari, Takayuki Nakanishi, Yasuchika Hasegawa, and Sarah L. Stoll

Chem. Mater., **Just Accepted Manuscript** • DOI: 10.1021/acs.chemmater.8b00393 • Publication Date (Web): 11 Apr 2018

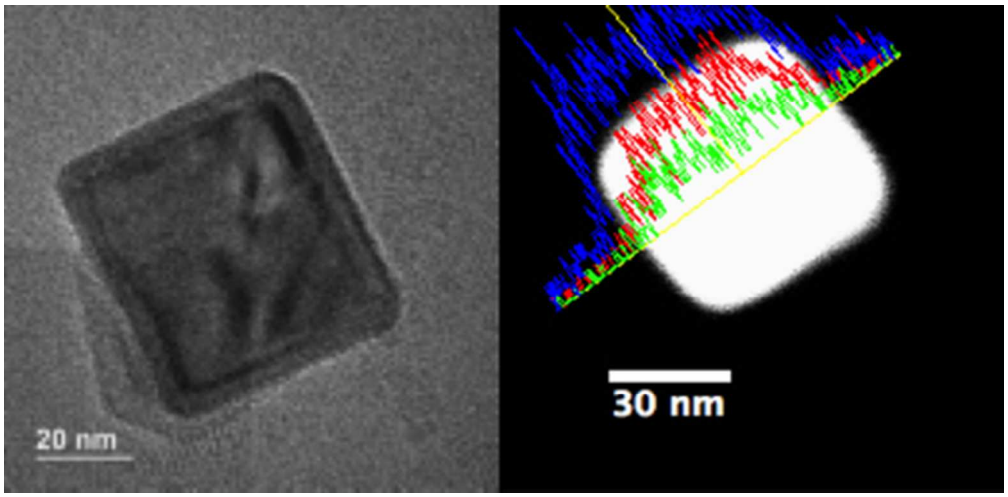

42x20mm (300 x 300 DPI)

Solid-State and Nanoparticle Synthesis of EuS_xSe_{1-x} Solid-Solutions

Haydee A. Dalafu, Nicholas Rosa, Derak James, Dane Asuigui, Michael McNamara, Akira Kawashima,[†] Shun Omagari,[†] Takayuki Nakanishi,[‡] Yasuchika Hasegawa,[†] and Sarah L. Stoll*

Department of Chemistry, Box 571227, Georgetown University, Washington D.C., USA 20057. Fax: 202-687-3964; Tel: 202-687-5839.

[†]Laboratory of Advanced Materials Chemistry, Division of Applied Chemistry Hokkaido University, N13W8, Kita-Ku, Sapporo, Hokkaido 060-8628, Japan

[‡]Department of Material Science and Technology, Tokyo University of Science, 6-3-1 Niijuku, Katsushika-ku, Tokyo, 125-8585, Japan

ABSTRACT

Europium chalcogenide alloys, EuS_xSe_{1-x}, have been synthesized in both the solid-state and as colloidal nanoparticles; and the composition, structure, magnetism, and optical band gaps have been characterized. The goal was to observe the consequences of selenium concentration on the electronic structure as evidenced by the optical and magnetic properties, and whether these properties are maintained in the nanomaterials. Both solid-state and nanoparticle alloys obey Vegard's law with a systematic change in cell constant as confirmed by the powder X-ray diffraction. The bulk materials form homogeneous alloys that exhibit a linear change in both magnetic and optical properties as a function of composition. A synthetic method to prepare nanoalloys with a wide range of S:Se ratio has been developed. The nanoalloys are homogeneous, and EDS mapping of single nanoparticles indicates relatively uniform S and Se composition across the nanocrystals. The magnetic properties of the nanoparticles appear to parallel those in the solid-state. Although the composition is an effective tool to tune to the optical band gap in the solid-state alloys with a linear change in E_g with composition, the nanoparticle optical band gaps appeared to be shifted, which we attribute to the presence of an amorphous selenium phase. The study of the properties of colloidal alloys highlights the importance of the mechanism of nanoparticle formation to control composition and purity.

INTRODUCTION

The europium chalcogenides comprise an unusual class of magnetic semiconductors that spans from ferromagnetism (EuO, EuS) to antiferromagnetism (EuTe).[1] In between, EuSe has a more complex magnetic phase diagram, exhibiting metamagnetism (antiferromagnetic at low fields and ferromagnetic at high fields) that reflects the close competition between ferro and antiferromagnetic coupling. The trend in properties are thought to be due to the Eu-Eu distances and changes in bonding down the periodic table that alter the electronic structure in systematic ways. The europium chalcogenides have been of interest because of the highly coupled magnetic, electronic, and optical properties, where a change in one can affect the others. As a result, they exhibit a range of properties including spin filtering effects,[2] giant magnetoresistance,[3] large magneto-optical Kerr rotations,[4] and the recently discovered giant magnetocaloric effects.[5,6] Each of these properties are notable for underlying fundamental questions in physics, and significantly, provide insight and inspiration for next generation solid-state devices with potential to use both spin and conductivity (spintronics) or to interconvert information between light, magnetism and conductivity.

Our initial studies of nanostructured EuS were motivated by the relationship between ferromagnetic coupling and the electronic band gap (E_g),[7] and the possibility to tune both using particle size.[8] The band gap (E_g) in europium chalcogenides has long been observed to correlate with magnetic properties and the ferromagnetic materials exhibit a shift in the E_g at the magnetic ordering temperature due to conduction band splitting.[9] The connection between the ferromagnetic ordering temperature, T_c, and the band gap has been modeled through the exchange integral J_1 (for ferromagnetic coupling), which decreases as the E_g increases.[10] Although decreasing the size of the EuS nanoparticles did decrease the ferromagnetic ordering temperature,[8] neither our group nor others have observed strong spectroscopic evidence of optical band gap changes with particle size.[11-15] We postulate this to be a consequence of the small estimated Bohr radius (< 2nm) and the difficulty in preparing very small nanoparticles. Band gap tuning arises from changes in the dispersion of the valence and conduction bands,[16] and the lack of size-dependent optical properties suggests modest changes to the density of states diagram. This could be because the band edge is defined by a ground state that even in the bulk is quite narrow (*f* band), or because the bonding is more ionic than related II-VI materials.

Solid solutions or composition alloys provide an alternative to particle size for tuning the band gap, particularly for applications where the optimized band gap requires very small

dimensions or quantum confinement is not observed. Semiconductor alloyed nanoparticles have gained attention as a promising method for tuning band gap and valence band energies.[17] Band gap tuning with constant nanoparticle size has been demonstrated for most II-VI semiconductors, including both cation alloys (e.g. $Cd_{1-x}Zn_xS$)[18] and anion alloys (e.g. $CdS_{1-x}Se_x$). [19] Both types of alloys exhibit composition-tunable emission. Importantly, alloys have become a useful tool for adjusting band edges to control the flow of electrons in materials of interest for solid-state devices including photovoltaics, such as the low-cost $Cu_2ZnSn(S_{1-x}Se_x)_4$[20] or PbS_xSe_{1-x}.[21] The variation in properties as a function of composition provides important insight into the bonding and band structure. For example, some semiconductors exhibit a simple linear change in E_g with composition. However, if the valence and conduction band energies are significantly off-set (or there is lattice mismatch),[22] the band gap can exhibit a 'bowed' effect as a function of composition. These differences connect the bonding and crystal chemistry to changes in the density of states. Generally, it appears that the alloyed nanoparticle optical band gaps parallel the same relationship with composition, whether linear or bowed, as the bulk materials.[23] There are no reports of the optical properties of bulk EuS_xSe_{1-x} alloys. The band gap of europium selenide (1.78 eV) is measurably larger than europium sulfide (1.65 eV), thus we were interested to see how the band gap varies as a function of composition and how the magnetic properties change.

We were motivated to synthesize the bulk EuS_xSe_{1-x} alloys to determine the optical properties, but the lack of optical data highlights the paucity of studies of europium chalcogenide alloys of any combination (S, Se, or Te). One of the advantages of investigating nanomaterials of EuS is the depth of the literature on the bulk solid-state material, which includes detailed measurements of the optical, electronic and magnetic properties.[24] These studies inform our understanding of nanoscale EuS. The limited investigations of alloys have been narrowly focused on magnetic studies as seen for $EuSe_{1-x}Te_x$,[25] and EuS_xSe_{1-x}.[26,27] Alloy composition is also used commonly to interrogate magnetocaloric materials,[28] and is of particular interest for EuS_xSe_{1-x} because of differences in the magnetic phase diagrams of the end members. It would be significant if composition may be used to simplify the complex magnetic phase diagram of EuSe, because it would aid in understanding the magnetocaloric effect in these materials. The order of the magnetic transitions, whether first order paramagnetic-ferromagnetic (seen in EuS),

or second order antiferromagnetic-ferromagnetic (like EuSe), has a strong effect on entropy change and refrigerant capacity.[29]

An important challenge for nanoscale synthesis is to translate the tools from the solid-state, such as doping and solid solutions, to nanoscale materials. This work also reports the first synthetic route to prepare EuS_xSe_{1-x} alloyed nanoparticles. The synthesis of EuS nanoparticles has been reported by several groups, [7,12,30-32] while Hasegawa[33,34] and others have lead the development of EuSe nanoparticles.[35,36] The use of the dithiocarbamate ligand as a source for the sulfur component and diphenyl-diselenophosphate for selenium were obvious choices given the demonstrated utility in the syntheses of the end members. However, we discovered these precursors presented challenges to forming alloys across the full composition range due to the differing reactivity of the S and Se precursors.

We believe the study of solid-state and nanoparticle materials is synergistic, and report here the solid-state synthesis of EuS_xSe_{1-x} from x =0-1 as well as the optical and magnetic properties of the bulk material as a function of composition. In addition, we have synthesized alloyed nanoparticles and provide detailed composition and structural characterization using X-ray diffraction and Transition Electron Microscopy (TEM), and Energy Dispersive Spectroscopy (EDS) of both line scans of single particles and elemental mapping of large collections of nanocrystals. While the magnetism corresponds well to solid-state alloys, our initial attempts to investigate the optical properties have been hindered by the presence of an amorphous impurity.

EXPERIMENTAL SECTION

Chemicals. Sulfur powder (99.998%), selenium powder (-100 mesh ≥99.5%), oleylamine (OLA, 70%, technical grade), hexadecylamine (HDA, 90%), 1-octadecene (ODE, 90%), diethylamine (>99.5%), diphenylphosphine (98%), diethylammonium di-ethyl, dithiocarbamate (97 %), 2,2'-bipyridine (99 %), and europium (III) chloride hexahydrate (99.9%) were purchased from Sigma-Aldrich. Europium powder (99.9%) was obtained from Alfa Aesar, sulfur powder (99.998%) and selenium powder (-100 mesh, ≥99.5%) were obtained from Sigma-Aldrich. All metals were kept in N_2 atmosphere glovebox and used as received.

Nanoparticle Precursors.

$Eu(S_2CNEt_2)_3Bpy$. Europium tris-diethyldithiocarbamate bipyridine, $Eu(DTC)_3Bpy$, was synthesized as reported previously. Briefly, Europium (III) chloride hexahydrate was dissolved in 2-propanol and added to a vigorously stirred solution of diethylammonium

diethyldithiocarbamate and 2,2'-bipyridine in acetonitrile at room temperature. The orange-red precipitate was collected via vacuum filtration and washed with ice-cold acetonitrile. FTIR: ν (C-N) = 1483 cm^{-1}, ν (C-S) = 997 cm^{-1}.

$[Et_2NH_2][Se_2PPh_2]$. The synthesis of diethylammonium diphenyldiselenophosphinate, or Et_2NH_2-DSP, was adapted from the analogous synthesis of $[(PhCH_2CH_2)_2PSe_2][R_2NH_2]$. Briefly, diphenylphosphine and selenium powder were mixed in dry, degassed EtOH under N_2 atmosphere. Diethylamine was added via syringe and the reaction heated to 60 ^oC for approximately 1 hour until the selenium powder had all reacted. The product precipitated upon cooling and was collected via vacuum filtration and washed with ice-cold Et_2O. FTIR; 1544 (w), 1433 (s), 1088 (m), 751(m), 691(m), 534(s), 514(s), 472(m), 450(m).

Eu(oleate)$_3$. was prepared following the procedure of Dickerson.[37] Briefly, Europium (III) chloride hexahydrate and three-equivalents of sodium oleate were dissolved in a mixture of 1:1:2 deionized water: ethanol: hexanes and refluxed for 4 hours. The organic phase was separated and washed three times with deionized water. Removal of the solvent under vacuum afforded Eu(oleate)$_3$ as a translucent solid. FTIR (ν cm^{-1}): 3005(w), 2923 (s), 2853 (sh), 1544, 1455, 1311, 722.

Solid-State Reactions of EuS_xSe_{1-x}. The quartz tubes (10 mm inner diameter) were purchased from Chemglass, and 8-inch long tubes closed by melting the quartz. The tubes were graphitized by wetting the inner walls with acetone and decomposing it by heating the tube using an acetylene/natural gas torch. In a N_2 glovebox, stoichiometric amounts of Eu powder, S powder, and Se powder were mixed and ground in an agate mortar and pestle to make 200 mg of powder. The graphitized quart tubes were charged with the powdered mixture and sealed under vacuum. The reactions were heated in a Lindberg/Blue M box furnace with the following heating profile: room temperature to 90˚C at 4˚C/min, 90˚C to 400˚C at 1˚C/min, 400˚C to 880˚C at 2˚C/min, maintain 880˚C for 48 hours, and finally cooled to room temperature at 7˚C/min. After the reaction, the tubes were broken open inside the glovebox and stored under N_2 atmosphere at all times.

Nanoparticle Reactions of EuS_xSe_{1-x}. In a 3-necked round bottom flask fitted with a thermocouple for temperature control and reflux condenser, hexadecylamine (2.5 g, 10.4 mmol) and 1-octadecene (5.0 mL, 25.1 mmol) were degassed under vacuum at 120°C for 1 hr. In a glovebox with a N_2 atmosphere, $Eu(Et_2NCS_2)_3Bpy$ (250 mg, 0.334 mmol), and different ratios of

DSP (11.1 mg, 0.027 mmol-75.6 mg, 0.181 mmol) were dissolved in 3.0 mL of oleylamine. The HAD/1-ODE solution was placed under N_2 and heated to 330°C and then the $Eu(Et_2NCS_2)_3Bpy$/DSP in oleylamine were injected via syringe. The color change was immediate upon injection, and the reaction was allowed to stir for 1 hr. The reaction was then cooled from 330°C to room temperature and hexanes introduced to disperse the nanocrystals and decanted into a centrifuge tube to remove solid hexadecylamine. Nanoparticles were precipitated with EtOH and collected by centrifugation at 4500 rpm for 10 minutes. The pellet was redispersed in hexanes and the precipitation and centrifugation procedure was repeated a total of 4 times to wash the nanocrystals. The nanoparticles were re-suspended in ~5 mL of hexanes.

Characterization. Powder X-ray diffraction (PXRD) patterns were collected on a Rigaku Ultima IV diffractometer equipped with a high-speed DTEX Silicon-strip detector using Cu Kα radiation at a scan speed of 1°/min, at 40 kV/44 mA. Cell constants were calculated from Rietveld refinements with GSAS-II. Samples were prepared for Transition Electron Microscopy by drop-casting nanoparticle samples dispersed in hexanes onto amorphous carbon-coated Cu grids. High-resolution TEM (HRTEM) and energy dispersive X-ray spectroscopy (EDS) analyses were performed on a JEOL JEM-2100F FEG TEM operated at 200 kV at the Advanced Imaging and Microscopy Lab in University of Maryland. Diffuse-reflectance UV-VIS spectra of solid-state bulk samples were obtained by diluting in PMMA using a Cary 5000 UV Vis-NIR spectrometer. The bandgap energies were determined by plotting ln(A) vs. energy (Urbach plot) and taking the intersection of the linear fits of the baseline and the absorption edge using MATLAB. ICP-MS measurements were conducted on diluted nitric acid digested samples of solid nanocrystals and was run on an Agilent 7700 series ICP-MS with Ar plasma. Magnetic Susceptibility was obtained on an MPS 3 SQUID magnetometer with field cooled samples at 1000 Oe for solid-state samples, or 5000 Oe for nanoparticles, from the Magnetic Measurement Facility of the University of South Carolina. The magnetic ordering temperature (theta) was determined by plotting 1/chi vs. T from 50 to 300 K and taking the x-intercept.

RESULTS/DISCUSSION

Solid-State Reactions. The solid-state synthesis of europium chalcogenides is facilitated by the simplicity of the Eu-S and Eu-Se phase diagrams.[38] Notably, the stability of the divalent state of

europium in the chalcogenide lattice reduces the number of potential impurity phases, and the relatively low melting point of europium (826°C) allows for simple silica sealed tube reactions. Few other compounds with close compositions exist, for example, Eu_2X_3 for X = S or Se do not appear in the phase diagrams. Although there is a stable mixed-valent Eu_3S_4[39] and a divalent metamagnetic $EuSe_2$ phase,[40] we have not observed either in any of our reactions. Care must be taken to exclude inadvertent oxygen, as small amounts can lead to oxychalcogenide (Eu_2O_2S/Se) impurities.[41,42] The conditions for the solid-state synthesis of the EuS-EuSe alloys was adapted from the literature,[43] and the products were crystalline and single-phased based on powder X-ray diffraction. A characteristic indication of alloying is that the cell constants vary linearly with composition, according to Vegard's law. As outlined by Hume Rothery rules, alloys or true solid solutions form when the end members are close in size, electronegativity, and valence.[44] Based on the systematic shift of the (200) peak, illustrated in Figure 1, the increase in selenium causes an increase in the cell constant as expected for the larger anion. The peak width and symmetry of the diffraction peaks indicate that the materials are homogeneous. The ICP-MS is challenging for the detection of sulfur,[45] so we used the ratio of Eu:Se to confirm composition and found that the compositions were often 2-4% higher in selenium than expected based on reactant stoichiometry. We attribute this to differences in volatility of the reagents. In Figure 2, the linear relationship between cell constant from GSAS refinement, plotted versus % selenium based on ICP, demonstrates that these materials follow Vegard's law. We include the data for this graph in a table that summarizes the ICP, and GSAS fits in Supporting Information (S1, as well as diffraction patterns in S2-S9).

The use of Vegard's law to confirm homogeneous alloy formation has been challenged by examples of thermoelectric materials that exhibited linear changes in cell constant as a function of composition but electron microscopy revealed the presence of nanostructured phase separation.[46] The nanostructuring supported the low thermal conductivity caused by phonon scattering by the nanostructure. Examples of nanostructuring include PbS-PbTe alloys, which is not surprising given the alloys exhibit a miscibility gap,[47] but also unexpectedly for PbS-PbSe.[48] This caught our attention as there are striking similarities between the lead and europium chalcogenides; both exhibit the sodium chloride structure type and the cell constants are remarkably close (EuS 5.97Å, PbS 5.94Å, EuSe 6.195 and PbSe 6.12Å, EuTe 6.598, PbTe 6.50 Å). In fact, this observation has led to many cation-alloy studies of the type $Pb_{1-x}Eu_xQ$ (Q = S,

Se, Te) investigated for magneto-optical properties and tuning the valence band of the lead chalcogenides.[49-51] After careful analysis, we do not believe this type of nanostructuring is present in the EuS_xSe_{1-x} alloys based on TEM. Because of the linearity of other physical properties, in addition to the cell constant, *vide infra*, we believe the EuS-EuSe materials form compositionally homogeneous solid solution alloys.

Magnetic Properties of Solid-State Alloys. The magnetic properties of the europium chalcogenides have been well studied and successfully modeled using a Heisenberg model for the spin structures. One would predict that the EuS_xSe_{1-x} alloys would have exchange integrals that systematically shift from EuS (J_1 = +0.21, J_2 = -0.11) to EuSe (J_1 = 0.11, J_2 = -0.09).[52] In simple terms, the coupling generally becomes weaker as the anion size increases with the ferromagnetic coupling (J_1) decreasing more rapidly than the antiferromagnetic coupling (J_2). The coupling is so close in EuSe that antiferromagnetic phases including NNSS and NSNS as well as NNS types have been reported at low temperatures and fields.[27] The exchange integrals have been proposed to be a function of cation-anion distance[53] as well as the band gap,[54] both of which increase from EuS (a = 5.96Å, Eg = 1.65 eV) to EuSe (a = 6.195Å, Eg = 1.78 eV). Interestingly, pressure studies of EuS and EuSe have found that ferromagnetic coupling greatly increases with pressure while the antiferromagnetic coupling is far less sensitive, which suggests that the band gap plays a greater role than distance in ferromagnetic coupling.[55] Previously, the magnetic properties of bulk alloys were reported for the chi-vs-temperature at a very low applied field of 80 Oe[56] which has the advantage that field-induced ferromagnetism may be neglected. This provides a simple measure for determining the composition where antiferromagnetic coupling becomes dominant. This work reported that the decrease in ferromagnetic coupling (as measured by Θ) for EuS_xSe_{1-x} was linear from x = 1-0.1, with a more complicated relationship for $x < 0.1$. We have adopted a similar approach and the data on bulk materials synthesized in our laboratory concur with these general observations. We observe a reasonably linear shift in the Θ from 16K to 8 K for compositions of EuS_xSe_{1-x} for x = 1-0.1, at fields of 1000 Oe, as shown in Figure 3. This linear relationship contrasts with another magnetic semiconductor: the class of chalcospinel of composition $CdCr_2S_{4-x}Se_x$, where the cell constant also obeys Vegard's law but there is a clear 'bowing' effect in Tc versus composition.[57] This raises questions as to the electronic structural differences between these two classes of magnetic semiconductors, and how these vary with composition. Our high selenium composition alloys appear to have a linear

increase in the Néel temperature, unlike that reported previously (see inset for Figure 3). This may be a consequence of the higher field used here. In the future, we are interested in investigating in greater detail how the concentration of sulfur influences the antiferromagnetic coupling and whether this can be used to remove various antiferromagnetic phases to determine the effect on the magnetic entropy.

Optical Properties of Solid-State Alloys. We were interested in the optical band gap as a function of composition to confirm whether the linear changes in the ferromagnetic ordering correlate with a linear change in E_g, or whether bowing is observed. The electronic structure of the europium chalcogenides is analogous to compound semiconductors with an anion-centered valence band and cation-centered conduction band. However, they are distinguished by having a narrow *f* band relatively close in energy above the anion band. As a result, the E_g has been reported as the energy difference between the *f* band to the conduction band. The band diagram for EuS and EuSe differ primarily in the width or dispersion of the conduction band, comprised of 5*d/6s* orbitals. Because there is decreased overlap the conduction band for EuSe is narrower leading to a larger energy separation or larger Eg. The changes to the width of the conduction band are systematic, leading to a regular change in the E_g (EuO < EuS < EuSe < EuTe). This is in contrast to the lead chalcogenides which exhibit an anomalous band gap behavior (E_g for PbS > Eg PbTe > Eg PbSe).[58] The absorption spectrum[59] for both single crystals and thin films of europium chalcogenides exhibit two transitions: the first corresponds to a 4*f* ($^8S_{7/2}$) to 5*d* (^7F_J multiplet) band followed closely by a second transition due to the 4*f* to 6*s* band.[60,61] To investigate the optical properties, we used room temperature UV-visible diffuse reflectance of powders. Our data for the solid-state alloys do not exhibit a pronounced energy minimum between the two absorption regions but both transitions are observed. Because the 4*f* band width is so narrow, the transition occurs between localized states and delocalized conduction band (5*d*/6*s*), thus the absorption edge has an exponential shape as described by the empirical Urbach relation.[61,62] We estimated the band gap using the intersection of 2 fitting lines to determine the onset of the absorption (see Supporting Information S12).[63] Based on this, as seen in Figure 4, the band gap shift appears to be linear from EuS to EuSe, supporting our conclusion that the bulk materials form true homogeneous alloys. The lack of bowing was of interest, and while there does not seem to be uniform agreement on the factors that contribute to the bowing parameter, differences in the cell constant (or lattice strain),[64,65] electronegativity,[66] and ionicity are

important considerations.[22,23] As argued for PbS_xSe_{1-x}, the small lattice mismatch supports the band gap linearity in the S-Se alloys, whereas a greater difference in cell constants would be expected to enhance bowing.[21] Although we have not investigated the temperature dependence of the absorption spectrum, it is possible to determine the room temperature Urbach energy, which reflects the effect of disorder on the band edge due to factors such as temperature, structure, and composition.[67] The energy follows the Urbach relation: $\alpha(\nu h) = \alpha_0 \exp(h\nu/E_u)$, where α_0 is a constant, $h\nu$ is the photon energy, and E_u is the Urbach energy. A plot of $\ln(\alpha)$ vs $h\nu$ can be fitted with a straight line, and the reciprocal of the slope of this linear region is E_u. We anticipated that the bulk materials would exhibit larger average Urbach energies for intermediate alloy compositions due to compositional disorder. Unfortunately, the Urbach energies determined from our diffuse reflectance data were fairly large, indicative of a broad absorption peak (~600 meV), with no trends in composition.

Nanoparticle Reactions. The synthesis of nanoscale EuS and EuSe both depend on the reduction of Eu(III) to Eu(II), using a chalcogenide-containing, ligand.[68] In the case of EuS nanoparticles, the synthesis employs a single source precursor, $Eu(S_2CNEt_2)_3Bpy$ in oleylamine (as the solvent and capping ligand). [12,31,32,69,70] Although oleylamine has been reported to be reducing,[71] we attribute the reduction of europium to the reducing ability of the dithiocarbamate ligand. One evidence to explain the oxidation-reduction chemistry is that the products of the solid-state thermolysis of $Eu^{3+}(S_2CNEt_2)_3Bpy$, produces reduced europium in $Eu^{2+}S$ as well as the oxidized ligand, dithiuram, as one of the products observed in the GCMS. The role of the ligand here is clear in that the reaction of tri-octylphosphine sulfide, or TOPS, with Eu(III) in oleylamine does not produce EuS. We have followed the debate on the formation of PbSe nanoparticles in which the reaction of $Pb(oleate)_2$ and TOPSe requires the presence of diphenylphosphine to form PbSe. The role of diphenyl phosphine has been proposed to be either to reduce lead[72] or, conversely, to promote the dissociation of the metal-oleate complex.[73] We note that Pb^0 has been observed (but only after the time to form nanoparticles)[73] and that the reduction of Cd^{2+} to Cd^0 has been proposed for reactions of $CdMe_2$ and R_3PE (E = S, Se, Te).[74] The role of the oxidation state is of interest for the formation of these metal chalcogenide nanoparticles,[75] and is relevant here given that the reduction potentials for Pb^{2+}/Pb^0 (E° = -0.126) and Cd^{2+}/Cd^0 (E° = -0.40) bracket the reduction potential for Eu^{3+}/Eu^{2+} (E° = -0.35 V).[76,77] One

might anticipate that reagents effective for these metals would be of utility for forming europium chalcogenides.

By contrast to EuS, the most commonly used ligand for the synthesis of EuSe is the di-phenyl-diselenophosphinate, $Ph_2PSe_2^-$ (R = phenyl). [78,79] O'Brien has pioneered the use of the dialkyl-diselenophosphinato complexes with transition metals as single source precursors to form a variety of nanomaterials.[80,81] Interestingly, depending on the analog of the ligand and the metal, either the transition metal selenide or phosphide can be produced.[82] To prepare EuSe nanoparticles, separate salts of europium and the di-selenophosphinate are injected together, because the stable $Eu(Se_2PPh_2)_3$ complex has been elusive in our hands (although it has been recently structurally characterized).[83] The *in situ* reaction of $KPPh_2$, Se, and $EuCl_3$ injected in hexadecylamine also leads to EuSe nanoparticles. These reactions clearly echo the chemistry observed in the formation of CdSe from the reaction of $Ph_2HP{=}Se$ with cadmium carboxylates in primary amines, in which $[Ph_2PSe_2]^-$ is observed.[84] An alternative ligand likely to lead to EuSe would be to use a di-selenocarbamate, $R_2NCSe_2^-$ structurally close to the dithiocarbamate. The di-selenocarbamate complexes have been prepared and used in nanoparticle synthesis;[85] however, this ligand requires the syntheses of CSe_2, which is both toxic and odorous.

Initially, we tested $Eu(acetate)_3$, and $Eu(oleate)_3$ with the appropriate ratio of the dithiocarbamate (DTC) and di-phenyl-diselenophosphinate (DSP) ligands in oleylamine to synthesize EuS-EuSe alloys. With europium acetate, the products were large, agglomerated, and based on the cell constant the selenium concentration was quite large. Elemental selenium was occasionally observed in the powder diffraction as an impurity in these reactions. The influence of acetic acid has been reported to increase the size of PbSe nanoparticles in an analogous way.[86] Another parallel with other metal chalcogenide nanoparticles syntheses is that the reactivity of the metal oleate is substantially slower, leading to longer reaction times and reduced nanoparticle yields.[75,87,88] Reactions of europium oleate with DTC and DSP produced only EuSe nanoparticles. In fact, the reaction of $Eu(oleate)_3$ and the dithiocarbamate ligand results in the formation of a purple solution, which we associate with the decomposition of precursor to the proposed EuS 'monomer', but no detectable EuS nanoparticles could be isolated. This may indicate that the reactivity of the precursor is unchanged but that the presence of oleate inhibits nanocrystal nucleation or growth. [74,89] Although these experiments demonstrate the importance

of the metal counter ion, acetate or oleate, we discarded both approaches because we were unable to synthesize sulfur rich nanoparticles alloys.

Nanoparticle Synthesis Control of S:Se. In order to access the full range of nanoparticle composition for nanoparticles of EuS_xSe_{1-x}, we employed the complex $Eu(S_2CNEt_2)_3Bpy$ as the europium and sulfur source with modest additions of the DSP ligand to obtain all of the alloy nanoparticles reported here. Although we assume the europium dithiocarbamate precursor has reactivity intermediate between the acetate and oleate, the Se in the product is still much greater than the relative concentration in solution due to the enhanced reactivity. The ability to form alloys from such mismatched ligands is unexpected as alloy composition control in nanoparticles has been found to be greatest when the anion precursor reactivity is balanced.[90] Generally, an empirical relationship has been observed between the amount of chalcogen in the nanoparticle product that is proportional to the precursor concentration and inversely related to the precursor-chalcogen bond energy.[92] Mechanistic studies of the dithiocarbamate precursors in nanoparticle syntheses have not been reported, but the studies of phosphine precursors is well developed. The rate of 'monomer' formation for II-VI nanoparticle syntheses increases in the order S < Se < Te, increasing with decreasing P-X bond strength.[91] A simple metric, the ^{31}P NMR chemical shifts (in addition to calculation), has been used to correlate the bond strength to reactivity.[92] The literature value for $Ph_2PSe_2^-$ (^{31}P δ = 24.02 ppm)[35] places it further upfield, corresponding to more reactive P-Se bonds than the previously investigated R_3P=Se derivatives, including TOP (tri-octylphosphine). Our chalcogenide ligands may not be comparable, given one has a C-S bond while the other P-Se, but our results are consistent with literature observation that the weaker precursor Se bond leads to higher reactivity.

Nanoparticle Alloy S:Se Composition. Given the differences in reactivity of the chalcogenide precursors, we were careful to look for evidence of composition variation in the nanomaterials. Based on the systematic shift in the cell constant, both from GSAS refinements as well as the superposition of the 200 peaks (see Figure 5), we believe that the nanoparticles are homogenous, and obey Vegard's law. The composition of the alloyed nanoparticles was evaluated using the cell constants based on GSAS refinements, ICP of Eu:Se ratios, and composition maps using Energy Dispersive Spectroscopy (EDS) from TEM for large quantities of nanoparticles taken at low magnification (Table 1). For the nanoparticles reported here, we only included samples for which the EDS of large nanocrystal collections were within 2-5% of the EDS composition line

scans of individual nanocrystals, and within 2-5% of selenium composition determined by the refinement of cell constants. A comparison of the EDS from elemental mapping (Table 1) with EDS from individual nanocrystals and ICP-MS can be found in Table S13 (Supporting Information). Because the cell constants of EuS (a = 5.97Å) and EuSe (a = 6.20 Å) are so close, small errors in the refinement translates to a large variation in composition. The ICP-MS disclosed that several samples had anomalously large amounts of selenium compared to the refined cell constant. We believe the excess selenium to be amorphous elemental material given there was no evidence of an impurity in the PXRD. The powder X-ray diffraction patterns for all of the nanoalloys can be found in Supporting Information (S12-16).

Single Particle Composition. Homogenously alloyed nanoparticles are most frequently distinguished from gradient alloys or core-shell structures based on the peak shape of the photoluminescence, which we have not observed in our materials. Alternatively, the peak shape of the powder X-ray diffraction should also be narrow and symmetric for homogenous alloys, and the metric used here. As a comparison, using the 200 peaks the average FWHM (0.25°) of our nanoparticle alloys were systematically wider than the bulk materials (average FWHM of 0.16°). The diffraction data gave Scherrer sizes between 30-50 nm, which is smaller than found by TEM (30-100 nm depending on the synthesis). Although the nanoparticle peaks are broad, they appear to be highly symmetric with no evidence of overlapping closely related phases, which would lead to shoulders or asymmetry.[93]

The elemental mapping of individual particles in TEM provides another measure of composition, but we primarily used it to aid in distinguishing the products' internal structure as homogeneous, gradient, or core-shell in composition. To facilitate this, the synthetic reaction times were held to one hour to obtain large particles (50 nm to 200 nm) which allowed for detailed composition mapping and line scans. For example, in Figure 6, the elemental mapping in the TEM of 50 nm $EuS_{0.4}Se_{0.6}$ nanoparticles exhibit even distribution of both S and Se. In Figure 7, two different compositions, one with high sulfur (~$EuS_{0.82}Se_{0.18}$, left) and one with high selenium (~$EuS_{0.21}Se_{0.79}$, right), were compared using elemental line scans. For both high and low sulfur, the intensity was proportional to the composition as expected by the calculated cell constants. In addition, the composition of the S and Se are fairly even across the crystal, for all samples reported here. Similar data for all the nanoparticle alloys reported here are included in the Supporting Information (S18-S21). Based on the EDS of nanoparticles, europium

concentration was slightly but consistently greater than predicted from stoichiometry, with a ratio of Eu:(S+Se) that ranged from 1.05-1.39. Typically, when the ratio of cation:anion is unequal, the higher concentration element is thought to terminate the surface (scaling with size given the changes in surface area to volume ratio with small sizes).[94,95] In our case, we believe that the slightly higher europium ratio can be explained by a reduced amount of chalcogen due to oxidation at the surface.

Nanoparticle Magnetic Properties. The magnetic properties were investigated for three of the nanoparticle alloys to confirm that the Tc has a similar decrease as a function of Se composition as the solid-state samples. We used a higher applied field (5000 Oe), so that the potential presence of unalloyed EuSe would be detected. The presence of pure EuSe should add a ferromagnetic step in the susceptibility versus temperature at 5K, which we did not observe. The ferromagnetic ordering temperatures ranged from 15 K-9 K for compositions from 30-80% selenium. These data are included in Figure 3 superimposed with Tc-vs-composition for the solid-state materials. Although the data is more limited than for the bulk materials, they support two conclusions about the alloyed nanoparticles. A wide ferromagnetic transition would indicate nanoparticles with a wide range of composition, but in fact the transitions were sharp leading us to conclude that the composition was fairly narrow. A measure of the europium oxidation state is that the measured μ_{eff} should be close to 7.9 $\mu_{B,}$ the calculated value for Eu(II) S = 7/2. Based on our Curie-Weiss plots, the μ_{eff} values were somewhat reduced for the nanoparticles (6.89-7.21 μ_B) compared to the solid-state samples (7.3-7.9 μ_B), but reasonably close. This is consistent with our hypothesis that the surface of the nanoparticles is slightly oxidized. The linear variation of Tc for the nanoparticles, and the close correlation with the solid-state materials support our composition determination. The magnetic data also confirm there are no magnetic amorphous impurities. We did not investigate nanoparticles in the range EuS_xSe_{1-x} for x = 0-0.2, but we did measure the susceptibility versus temperature for pure EuSe nanoparticles and found a Néel temperature of approximately 5K as reported for bulk materials at high fields.

Nanoparticle Optical Properties. Typically, photoluminescence is the most widely used technique for unambiguously determining the optical bandgap; unfortunately, we do not observe luminescence in our nanomaterials. The lowest energy transition $4f^7$ to conduction band ($5dt_{2g}$) is indirect, weak, and broad, making the onset of absorbance challenging to determine. Rather than measure the UV-visible spectra of solution phase nanoparticles, where the large diameters

caused significant scattering, we dried the nanoparticles and measured the diffuse reflectance using the same preparation as for the bulk solid-state samples. The nanoparticle optical spectra were similar to the bulk solid- state samples; however, the absorption edges were found to be shifted on average to higher energies in the range of 1.74-1.94 eV. This was surprising, given that quantum confinement is unlikely in such large nanoparticles. There also was no systematic dependence on composition, as expected from the bulk materials. However, the excess of selenium from the ICP-MS of our nanoparticles led us to confirm the presence of elemental selenium in the nanoparticle samples. The most common impurity materials we have observed in the synthesis of the end members includes the oxychalcogenides (Eu_2O_2S or Eu_2O_2Se), or in the case of EuSe, elemental Se. The oxychalcogenides have quite large band gaps (oxysulfides,[96] E_g>4.4 eV, oxyselenides[97] have been calculated to be E_g > 3.5 eV), and seemed unlikely to be responsible for shifts in this low energy peak. However, Raman spectroscopy allowed for a definitive identification of elemental selenium; two samples had amorphous selenium with weak, broad peak near 250 cm^{-1}, while three samples had the 235 cm^{-1} (A mode) of trigonal selenium and the sample with most Se impurity based on ICP also exhibited the weak 143 cm^{-1} (E mode) peak as noted in Table 1.[98] The range of E_g for nanoparticles of trigonal Se (1.6 eV-1.99 eV depending on the morphology),[99-101] is unfortunately quite close to the range of band gap for the EuS-EuSe alloys (1.65 eV-1.78 eV). Similar discrepancies in the band gap energy of $Cu_2ZnSnSe_4$ materials have been reported for materials that appear phase pure by powder X-ray diffraction contain small amounts of ZnSe impurity.[102]

Nanoparticle Formation. The question of whether the nanoparticles are homogeneous alloys or not has implications for the physical properties measured and also for the mechanism of nanoparticle formation, an important area of investigation. We have been unable to study the detailed formation of monomer, nucleation and growth, using *in situ* photoluminescence as commonly done for II-VI nanoparticles (our materials do not exhibit photoluminescence). However, we can make some inferences based on analysis of our products. When the anion reactivity is not balanced, the mismatch in reactivity often leads to gradient alloys, as observed in CdSeTe nanoparticles.[23] The composition can be homogenized by heating above some distinct 'alloying temperature' for cation alloys.[103] In order to gain insight into the formation of the alloyed nanoparticles, we have plotted the percent composition (i.e. (Se/S + Se)*100) of selenium in the product versus the percent Se in the reactants as shown in Figure 7. Clearly, very

small increases in solution selenium cause a large incorporation of Se in the product composition. This curve is similar to that observed for PbSe-PbTe nanoparticle alloys in that solution concentrations of the more reactive Te precursor between 0-20% produces products with the full range of Te up to PbTe.[90] One of the challenges with the alloys of lead chalcogenides is that both particle size and composition affect E_g, while for the europium chalcogenides, we have shown that the optical properties are only a function of composition. However, the presence of the Se impurity is a concern for interpreting the optical data of the nanoparticles. The need for pure alloyed nanoparticles provides motivation to further elucidate the mechanism of nanoparticle formation in the europium chalcogenides.

The focus of nanoparticle mechanistic studies is dominantly on the chalcogenide precursor because the metal concentration can be independently controlled.[73,104] In fact, kinetic control over ligand decomposition has been highly successful in producing remarkable size control for a wide range of nanoparticles.[105,106] Much of the mechanistic data can be fit into the La Mer mechanism of nucleation and growth, which is distinct from Ostwald ripening in that the reaction rate depends on three steps: precursor reaction, nucleation, and nanocrystal growth.[107] However, we note that unlike the EuS and EuSe nanoparticles we have investigated, we observe some Eu-S-Se nanomaterials that are more rectangular than cubic, which may indicate aggregative nanocrystal growth.[108] One of the challenges here is that the ligands must be able to reduce the Eu(III), limiting the classes of potential reagents. Although we observe many similarities with the synthesis of II-VI semiconductor nanoparticles, an important distinction is the reduction chemistry of europium and whether the environment can be manipulated to control this. We believe this is key to the formation of europium chalcogenide alloyed nanoparticles, and also key to the synthesis of new divalent lanthanide nanomaterials.

CONCLUSIONS

The solid-state synthesis of bulk EuS_xSe_{1-x} alloys from the elements leads to highly crystalline and pure alloys. The properties of these materials change as expected in terms of cell constants that increase with increasing the larger Se anion, as well as systematic variation in ferromagnetic magnetic coupling and optical properties. The band gap as a function of composition was determined to be linear, indicating that the band structures of the two materials, EuS and EuSe, are minimal. Based on the evidence from bulk materials, we anticipate that it should be possible to select the optical band gap or magnetic coupling in the nanoparticle alloys

by targeting a specific S:Se ratio. We believe that the presence of elemental selenium impedes analysis of the optical band gap of the nanomaterials. Although our synthetic method is the first to demonstrate EuS_xSe_{1-x} alloyed nanomaterials, greater synthetic control, without impurities, will be required to prepare nanoparticle alloys with a distinct range of band gap. The analysis of our materials leads us to believe that the nanoparticle alloys are homogeneous, but it raises questions as to the rate of monomer formation, nucleation, and whether a wider range of chalcogen sources might lead to better-matched reactivities and, thus, more controlled compositions.

ACKNOWLEDGMENT. We thank the National Science Foundation for funding this work, in several ways, foundational work (CHE:1112387) and currently CHE-1607905, as well as through the REU program CHE-REU 1156788, and the EAPSI program CHE-1515396. The author thanks Michelle Regulacio for her early work on this project.

Supporting Information Available. A Table of the ICP, Cell constant and GSAS wR, and GOF for the solid-state samples is in S1. In addition, the powder diffraction data for solid-state (S2-S9) and nanoparticle alloys (S13-S17), the fitting procedure for the optical spectra (S11), the magnetic susceptibility data (S10) as well as a summary of the elemental anlaysis of the nanocrystals by ICPMS, EDS composition maps and line scans of individual nanocrystals are summarized in Table 2 in S12. Finally, the EDS for all other nanoparticle samples are in S18-21. The Raman spectra of $EuS_{0.4}Se_{0.6}$ is included in S22. Histograms of nanoparticle diameters are in S23-S28. This material is available free of charge via the Internet at http://pubs.acs.org.

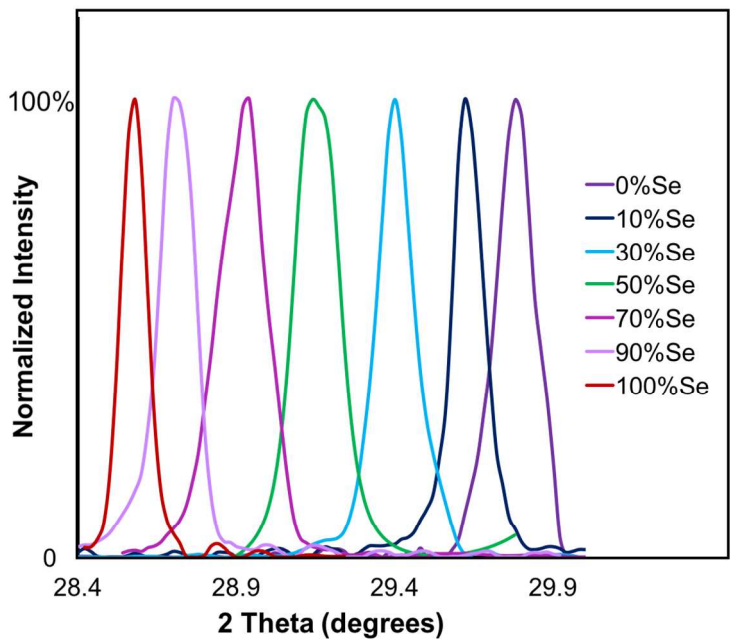

Figure 1. Powder X-ray diffraction peaks of the 200 peaks for solid-state EuS_xSe_{1-x}.

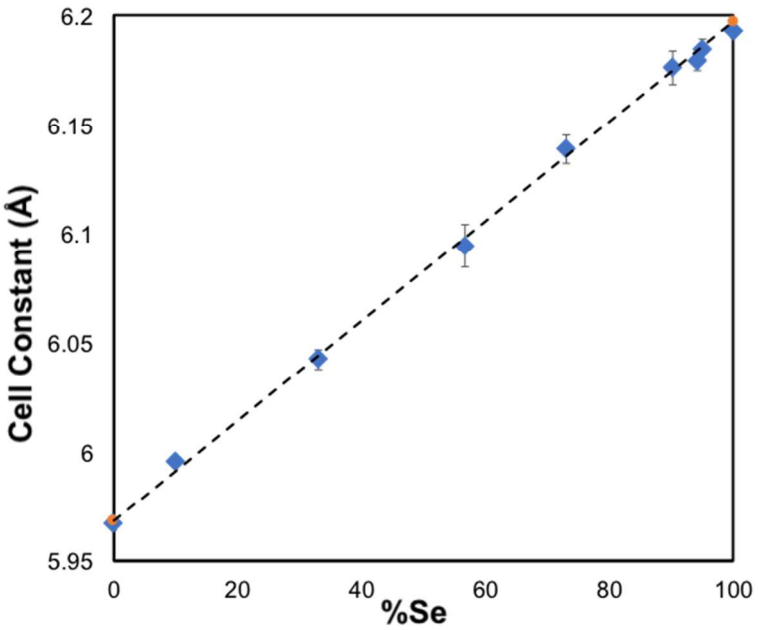

Figure 2. Cell constants from GSAS refinement vs. % Se precursor from solid phase synthesis.

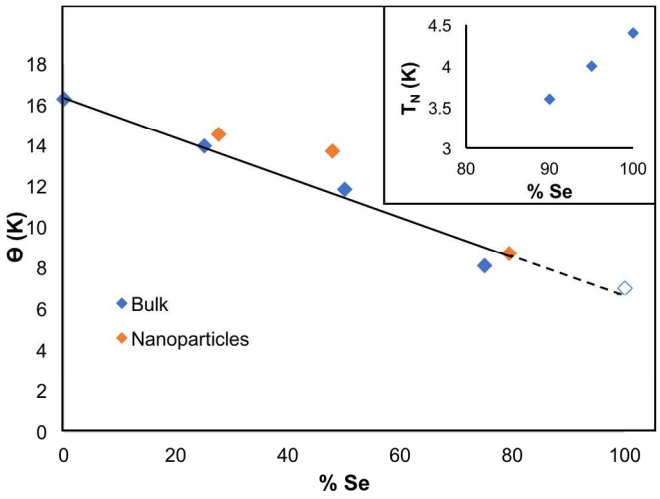

Figure 3. Theta versus composition for bulk (blue) and nanoparticle (red) EuS_xSe_{1-x}.

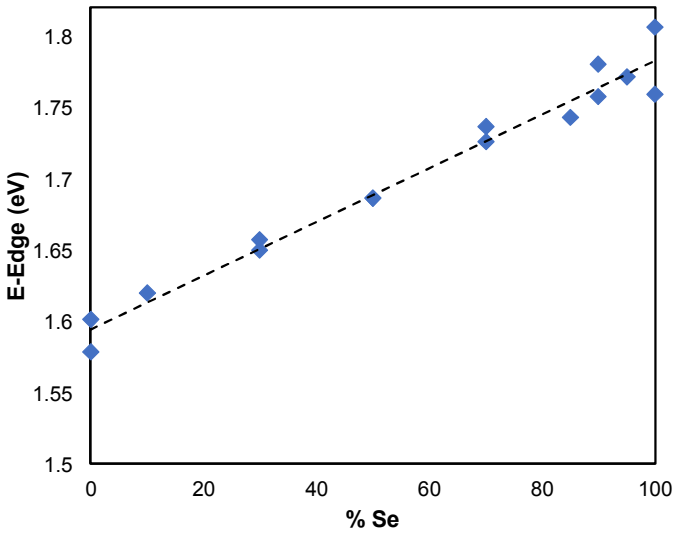

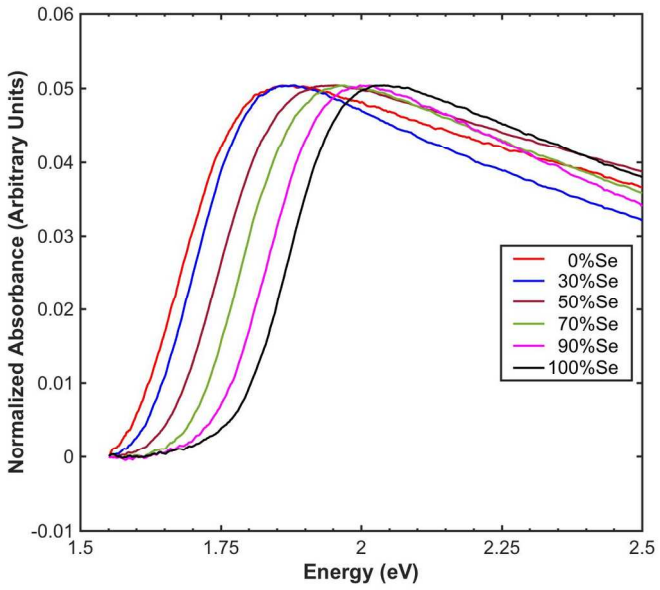

Figure 4. Plot of bandgap (eV) vs composition for solid-state bulk samples.

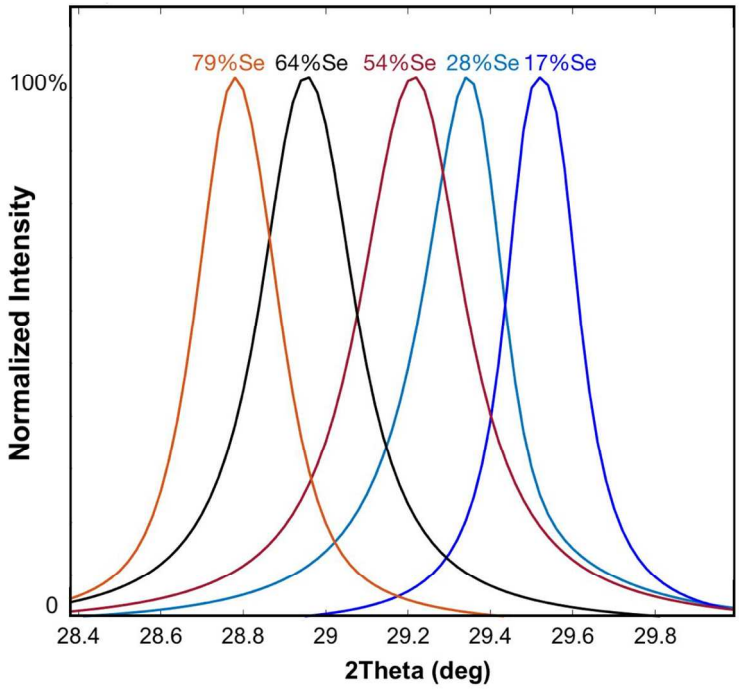

Figure 5. Powder X-ray diffraction peaks of the 200 peaks for colloidal EuS-EuSe alloys.

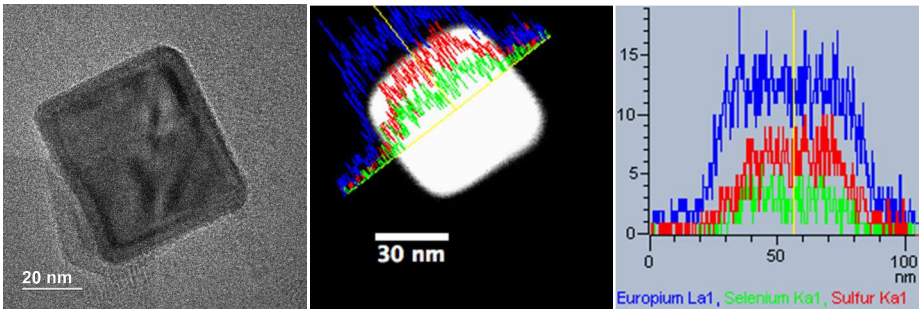

Figure 6. TEM image and EDS line scans of $EuS_{0.82}Se_{0.18}$ nanoparticle NR536.

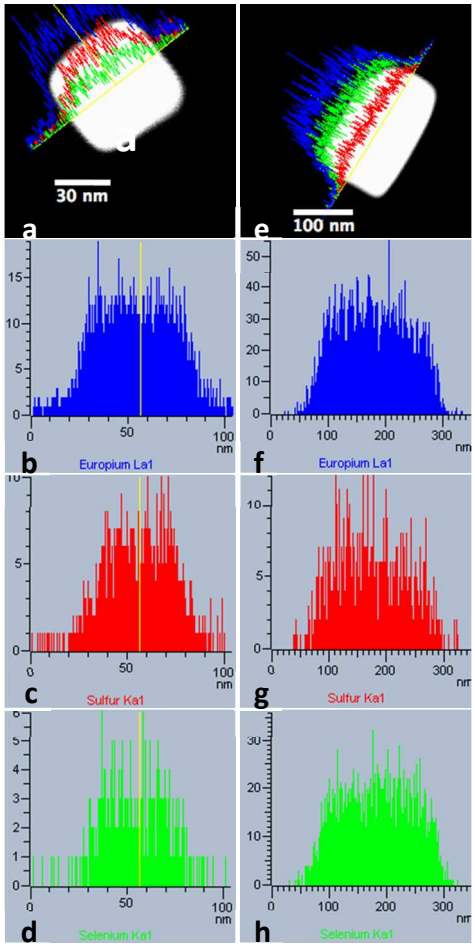

Figure 7. EDS Eu, S and Se line scans for EuS_xSe_{1-x} nanoparticles for x = 0.82 (a-d) NR536, and x = 0.21 (e-h) NR551.

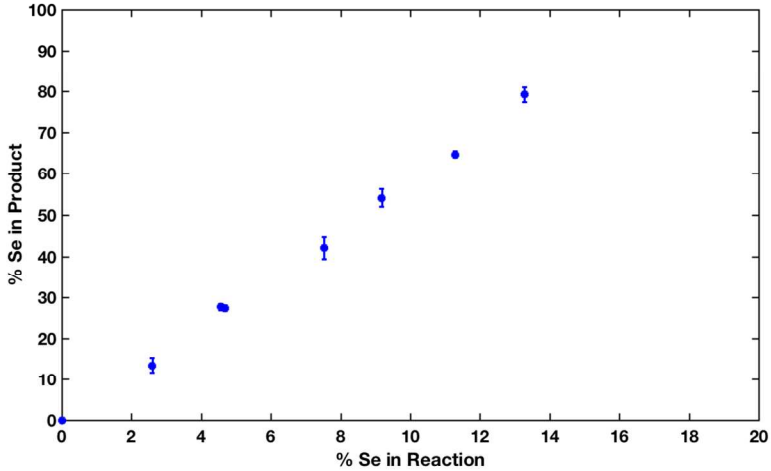

Figure 8. Composition of colloidal alloys with percent Se in reaction where %Se is defined as (Se/(S+Se)*100).

Table 1. Summary of reactant and product composition in EuSSe nanoparticles

Sample	%Se react	%Se ICP	Eu:S+Se EDS	%Se EDS	%Se GSAS	Cell Constant (Å)	wR (%)	GOF	Scherrer Size (nm)	Eg (eV)
NR544	2.6	23.1	1.3	13(2)	14.5(1)	6.002(2)	2.83	2.5	41	1.74
NR536	4.6	37.9	1.05	28(2)	27.9(1)	6.031(3)	3.43	3	30	1.78*
NR545	7.5	49.8	1.15	48(2)	44.8(2)	6.072(4)	3.13	2.6	34	1.77
NR549	9.2	61.5	1.39	54(3)	55.2(2)	6.120(5)	2.97	2.3	28	1.78*
NR550	11.0	143.6	1.13	64(2)	67.1(2)	6.124(4)	3.13	2.8	30	1.88*
NR551	13.3	94.1	1.2	79(2)	78.7(1)	6.151(3)	2.45	1.9	37	1.94*

*Exhibited presence of trigonal Se.

REFERENCES

1. McGuire, T.; Shafer, M. "Exchange Interactions in Compounds Ferromagnetic Europium Compounds" *J. Appl. Phys.* **1964**, *35*, 984–988.

2. Moodera, J. G. S.; Santos, T. S.; Nagahama, T. "The Phenomena of Spin-Filter Tunnelling" *J. Phys.: Condens. Matter* **2007**, *19*, 165202 (1-24).

3. Molnar, von, S.; Methfessel, S. "Giant Negative Magnetoresistance in Ferromagnetic $Eu_{1-x}Gd_xSe$". *J. Appl. Phys.* **1967**, *38*, 959–964.

4. Greiner, J. H., "Longitudinal magneto-optical Kerr Effect Longitudinal magneto-optical Kerr effect in EuO and EuS" *Appl. Phys. Lett.* **1966**, *9*, 27-29.

5 . Li, D. X.; Yamamura, T.; Nimori, S.; Homma, Y.; Honda, F.; Haga, Y.; Aoki, D. "Large Reversible Magnetocaloric Effect in Ferromagnetic Semiconductor EuS" *Solid State Communications* **2014**, *193*, 6–10.

6. Li, D. X.; Yamamura, T.; Nimori, S.; Homma, Y.; Honda, F.; Aoki, D. "Giant and Isotropic Low Temperature Magnetocaloric Effect in Magnetic Semiconductor EuSe" *Appl. Phys. Lett.* **2013**, *102*, 152409-1–152409-4.

7. Regulacio, M. D.; Bussmann, K.; Lewis, B.; Stoll, S. L. "Magnetic Properties of Lanthanide Chalcogenide Semiconducting Nanoparticles" *J. Am. Chem. Soc.* **2006**, *128*, 11173–11179.

8. Regulacio, M. D.; Kar, S.; Zuniga, E.; Wang, G.; Dollahon, N.; Yee, G.; Stoll, S. "Size-Dependent Magnetism of EuS Nanoparticles" *Chem. Mater.* **2008**, *20*, 3368–3376.

9. Freiser, M. J.; Holtzberg, F.; Methfessel, S.; Pettit, G.; Schafer, M.; Suits, J. C. "The Magnetic Red Shift in Europium Chalcogenides" *Z. Helvetica Physica Acta Band* **1968**, *41*, 832–838.

10. Zinn, W. Session 2: "Magnetic Properties and Interactions" *J. Magn. Magn. Mat.* **1976**, *3*, 23–36.

11. Thongchant, S.; Hasegawa, Y.; wada, Y.; Yanagida, S. "Liquid-Phase Synthesis of EuS Nanocrystals and Their Physical Properties" *J. Phys. Chem. B* **2003**, *107*, 2193–2196.

12. Mirkovic, T.; Hines, M. A.; Nair, P. S.; Scholes, G. D. "Single-Source Precursor Route for the Synthesis of EuS Nanocrystals" *Chem. Mat.* **2005**, *17*, 3451–3456.

13. Zhao, F.; Sun, H.-L.; Su, G.; Gao, S. "Synthesis and Size-Dependent Magnetic Properties of Monodisperse EuS Nanocrystals" *Small* **2006**, *2*, 244–248.

14. Selinsky, R. S.; Keavney, D. J.; Bierman, M. J.; Jin, S. "Element-Specific Magnetometry of EuS Nanocrystals" *Appl. Phys. Lett.* **2009**, *95*, 202501.

15. Redígolo, M. L.; Koktysh, D. S.; Rosenthal, S. J.; Dickerson, J. H.; Gai, Z.; Gao, L.; Shen, J. "Magnetization Reversal in Europium Sulfide Nanocrystals". *Appl. Phys. Lett.* **2006**, *89*, 222501.

16. Alivisatos, A.P. "Perspectives on the Physical Chemistry of Semiconductor Nanocrystals" *J. Phys. Chem.* **1996**, *100*, 13226-13239.

17. Regulacio, M. D.; Han, M.-Y. "Composition-Tunable Alloyed Semiconductor Nanocrystals" *Acc. Chem. Res.* **2010**, *43*, 621–630.

18. Zhong, X. H.; Han, M. Y.; Dong, Z. L.; White, T. J.; Knoll, W. "Composition-tunable $Zn_xCd_{1-x}Se$ nanocrystals with high luminescence and stability". *J. Am. Chem. Soc.* **2003**, *125*, 8589–8594.

19. Swafford, L. A.; Weigand, L. A.; Bowers, M. J.; McBride, J. R.; Rapaport, J. L.; Watt, T. L.; Dixit, S. K.; Feldman, L. C.; Rosenthal, S. J. "Homogeneously alloyed CdS_xSe_{1-x} nanocrystals: Synthesis, characterization, and composition/size-dependent band gap". *J. Am. Chem. Soc.* **2006**, *128*, 12299–12306.

20. Riha, S. C.; Parkinson, B. A.; Prieto, A. L. "Compositionally Tunable $Cu_2ZnSn(S_{1-x}Se_x)_4$ Nanocrystals: Probing the Effect of Se-Inclusion in Mixed Chalcogenide Thin Films". *J. Am. Chem. Soc.* **2011**, *133*, 15272–15275.

21. Ma, W.; Luther, J. M.; Zheng, H.; Wu, Y.; Alivisatos, A. P. "Photovoltaic Devices Employing Ternary PbS_xSe_{1-x} Nanocrystals" *Nano Lett.* **2009**, *9*, 1699–1703.

22. Tit, N.; Obaidat, I. M.; Alawadhi, H. "Origins of Bandgap Bowing in Compound-Semiconductor Common-Cation Ternary Alloys". *J. Phys.: Condens. Matter* **2009**, *21*, 075802–075807.

23. Bailey, R. E.; Nie, S. "Alloyed Semiconductor Quantum Dots: Tuning the Optical Properties Without Changing the Particle Size" *J. Am. Chem. Soc.* **2003**, *125*, 7100–7106.

24. Wachter, P., *Handbook on the Physics and Chemistry of Rare Earths*, North-Holland Publishing Co. 1979, Volume 2, Chapter 19.

25. Hihara, T.; Kojima, K.; Kamigaichi, T. "NMR Study of Hyperfine Fields at 153Eu in $EuSe_{1-x}Te_x$ with $X < 0.1$" *J. Phys. Soc. Jap.* **1981**, *50*, 1499–1504.

26. Kato, I.; Keneko, Y.; Mitani, T.; Koda, T. "Magnetic Ordering of $EuS_{1-x}Se_x$" *J. Phys. Soc. Japan* **1979**, *47*, 1367–1368.

27. Kojima, K.; Hihara, T.; Kamigaichi, T. "Magnetic Phases of $EuSe_{1-x}S_x$ with X <0.3" *J. Phys. Soc. Jpn.* **1980**, *49*, 2419–2420.

28. Shen, B. G.; Sun, J. R.; Hu, F. X.; Zhang, H. W.; Cheng, Z. H. "Recent Progress in Exploring Magnetocaloric Materials" *Adv. Mater.* **2009**, *21*, 4545–4564.

29. Pecharsky, V. K.; Gschneidner, K. A. "Magnetocaloric Effect From Indirect Measurements: Magnetization and Heat Capacity" *J. Appl. Phys.* **1999**, *86(1)*, 565-575.

30. Thongchant, S.; Hasegawa, Y.; Wada, Y.; Yanagida, S. "Liquid-Phase Synthesis of EuS Nanocrystals and Their Physical Properties" *J. Phys. Chem. B* **2003**, *107*, 2193–2196.

31. Redígolo, M. L.; Koktysh, D. S.; van Benthem, K.; Rosenthal, S. J.; Dickerson, J. H. "Europium Sulfide Nanoparticles in the Sub-2nm Size Regime" *Mater. Chem. Phys.* **2009**, *115*, 526–529.

32 Zhao, F.; Sun, H.-L.; Su, G.; Gao, S. "Synthesis and Size-Dependent Magnetic Properties of Monodisperse EuS Nanocrystals" *Small* **2006**, *2*, 244–248.

33. Hasegawa, Y.; Adachi, T.-A.; Tanaka, A.; Afzaal, M.; O'Brien, P.; Doi, T.; Hinatsu, Y.; Fujita, K.; Tanaka, K.; Kawai, T. "Remarkable Magneto-Optical Properties of Europium Selenide Nanoparticles with Wide Energy Gaps". *J. Am. Chem. Soc.* **2008**, *130*, 5710–5715.

34. Tanaka, A.; Adachi, T.-A.; Hasegawa, Y.; Kawai, T. "Crystal Growth of Nanoscaled Europium Selenide Having Characteristic Crystal Shapes" *J. Alloys Compd.* **2009**, *488*, 538–540.

35. Wang, C.; Zhang, D.; Xu, L.; Jiang, Y.; Dong, F.; Yang, B.; Yu, K.; Lin, Q. "A Simple Reducing Approach Using Amine to Give Dual Functional EuSe Nanocrystals and Morphological Tuning" *Angew. Chem. In. Ed.* **2011**, *50*, 7587–7591.

36. Wang, C.; Xu, L.; Li, X.; Lin, Q. "Divalent Europium Nanocrystals: Controllable Synthesis, Properties, and Applications" *Chem PhysChem.* **2012**, *13*, 3765–3772.

37. Mahajan, S. V.; Dickerson, J. H. "Synthesis of Monodisperse Sub-3 Nm RE_2O_3 and Gd_2O_3:RE^{3+} Nanocrystals" *Nanotechnology* **2007**, *18*, 325605–325606.

38. Massalski, T. B., Okamoto, H.; Subramanian, P.R.; Kacprzak, L., "Binary Phase Diagrams", 2nd Ed. ASM International, Ohio 1990.

39. Pott, R.; Güntherodt, G.; Wichelhaus, W.; Ohl, M.; Bach, H. "Thermal Properties of Eu_3S_4: Order-Disorder Transition" *Phys. Rev. B* **1983**, *27*, 359–363.

40. Aitken, J. A.; Cowen, J. A.; Kanatzidis, M. G. "Metamagnetic Transition in $EuSe_2$: a New, Metastable Binary Rare-Earth Polychalcogenide" *Chem. Mater.* **1998**, *10*, 3928–3935.

41. Llanos, J.; Sanchez, V.; Mujica, C.; Buljan, A. "Synthesis, Physical and Optical Properties, and Electronic Structure of the Rare-Earth Oxysulfides Ln_2O_2S (Ln=Sm, Eu)" *Mater. Res. Bull.* **2002**, *37*, 2285–2291.

42. Guittard, M.; Flahaut, J.; Domange, L. "The Complete Series of Oxyselenides of Rare Earths and Yttrium" *Acta Cryst,* **1966**, *21*, 832.

43. Kaldis, E. "High Temperature Vapour Phase Growth of Europium Sulphide, Selenide and Telluride" *J. Cryst. Growth* **1968**, *3-4*, 146–149.

44. Hume-Rothery, W. "Phase Stability in Metals and Alloys"; Rudman, P. S., Stringer, J., Jaffee, R. I., Eds.; McGraw-Hill: New York, 1976.

45. Moreels, I.; Lambert, K.; Smeets, D.; De Muynck, D.; Nollet, T.; Martins, J. C.; Vanhaecke, F.; Vantomme, A.; Delerue, C.; Allan, G.; "Size-Dependent Optical Properties of Colloidal PbS Quantum Dots" *ACS Nano* **2009**, *3*, 3023–3030.

46. Sootsman, J. R.; Chung, D. Y.; Kanatzidis, M. G. "New and Old Concepts in Thermoelectric Materials" *Angew. Chem. Int. Ed.* **2009**, *48*, 8616–8639.

47. Volykhov, A. A.; Yashina, L. V.; Shtanov, V. I. "Phase Relations in Pseudobinary Systems of Germanium, Tin, and Lead Chalcogenides" *Inorg. Mat.* **2006**, *42*, 596–604.

48. Androulakis, J.; Todorov, I.; He, J.; Chung, D. Y.; Dravid, V.; Kanatzidis, M. "Thermoelectrics From Abundant Chemical Elements: High-Performance Nanostructured PbSe–PbS" *J. Am. Chem. Soc.* **2011**, *133*, 10920–10927.

49. Bauer, B.; Pascher, H.; Zawadzki, W. "Magneto-Optical Properties of Semi-magnetic Lead Chalcogenides" *Semiconductor Sci. Technol* **1992**, *7*, 703–723.

50. Tomm, J.; Mollmann, K.; Peuker, F.; Herrmann, K.; Bottner, H.; Tacke, M. "Valence Band Hybridizing in Europium-Alloyed Lead Selenide" *Semicond. Sci. Techno.* **1994**, *9*, 1033–1041.

51. Krenn, H.; Herbst, W.; Pascher, H.; Ueta, Y.; Springholz, G.; Bauer, G. "Interband Faraday and Kerr Rotation and Magnetization of $Pb_{1-x}Eu_xTe$ in the Concentration Range $0<X<1$" *Phys. Rev. B* **1999**, *60*, 8117–8128.

52. Zinn, W. "Microscopic Studies of Magnetic Properties and Interactions Recent Results on Europium-Monochalcogenides" *J. Magn. Magn. Mater.* **1976**, *3*, 23–36.

53. Passell, L.; Dietrich, O.; Als-Nielsen, J. "Neutron Scattering From the Heisenberg Ferromagnets EuO and EuS, the Exchange Interactions" *Phys. Rev. B* **1976**, *14*, 4897–4907.

54. Wachter, P., "The Optical, Electronical and Magnetic Properties of the Europium Chalcogenides and the Rare-Earth Pnictides" *Critical Reviews in Solid State Sciences*, **1972**, *3*(2), 189-241.

55. Goncharenko, I.; Mirebeau, I. "Ferromagnetic Interactions in EuS and EuSe Studied by Neutron Diffraction at Pressures Up to 20.5 GPa" *Phys. Rev. Lett.* **1998**, *80*, 1082-1085.

56. Guittard, M.; Flahaut, J.; Domange, L. "The Complete Series of Oxyselenides of Rare Earths and Yttrium" *Acta Cryst,* **1966**, *21*, 832.

57. Borukhovich, A.; Marunya, M.; Bamburov, V. "Peculiarities of the Magnetic Phase Transition" *Sov. Phys. JETP* **1976**, *44*, 567–570.

58. Scanlon, W. "Recent Advances in the Optical and Electronic Properties of PbS, PbSe, PbTe and Their Alloys" *J. Phys. Chem. Solids* **1958**, *8*, 423–428.

59. Güntherodt, G.; Schoenes, J.; Wachter, P. "Optical Constants of the Eu Chalcogenides Above and Below the Magnetic Ordering Temperatures" *J. Appl. Phys.* **1970**, *41*, 1083–1084.

60. Wachter, P., '*Europium chalcogenides: EuO, EuS, EuSe and EuTe*" *Handbook on the Physics and Chemistry of Rare Earths*, Ed. Gschneidner, K., Eyring, L.; North-Holland Publishing Co. **1979**, Ch. 19, p. 507-574.

61. Schoenes, J. "Magneto-Optic and Electronic Structure of the Magnetically Ordering Europium Chalcogenide" *Z. Physik* **1975**, *20*, 345–368.

62. Guerra, J. A.; Montañez, L.; De Zela, F.; Winnacker, A.; Weingärtner, R. "On the Origin of the Urbach Rule and the Urbach Focus" *MRS Proc.* **2013**, *1536*, 139–145.

63. Xu, J.; Yang, X.; Wang, H.; Chen, X.; Luan, C.; Xu, Z.; Lu, Z.; Roy, V. A. L.; Zhang, W.; Lee, C.-S. "Arrays of ZnO/$Zn_xCd_{1-x}Se$ Nanocables: Band Gap Engineering and Photovoltaic Applications" *Nano Lett.* **2011**, *11*, 4138–4143.

64. Cade, N. "Band Bowing in Semiconductor Alloys and Superlattices" *Semicond. Sci. Technol.* **1987**, *2*, 255–260.

65. Singh, D. J.; Xu, Q.; Ong, K. P. "Strain Effects on the Band Gap and Optical Properties of Perovskite $SrSnO_3$ and $BaSnO_3$" *Appl. Phys. Lett.* **2014**, *104*, 011910–011914.

66. Aminorroaya Yamini, S.; Patterson, V.; Santos, R. "Band-Gap Nonlinearity in Lead Chalcogenide (PbQ, Q = Te, Se, S) Alloys" *ACS Omega* **2017**, *2*, 3417–3423.

67. Kranjčec, M.; Studenyak, I. P.; Kurik, M. V. "Urbach Rule and Disordering Processes in $Cu_6P(S_{1-x}Se_x)_5Br_{1-y}I_y$ Superionic Conductors" *J. Phys. Chem. Solids* **2006**, *67*, 807–817.

68. Boncher, W.; Dalafu, H.; Rosa, N.; Stoll, S. "Europium Chalcogenide Magnetic Semiconductor Nanostructures" *Coord. Chem. Rev.* **2015**, *289-290*, 279–288.

69. Hasegawa, Y.; Afzaal, M.; O'Brien, P.; Wada, Y.; Yanagida, S. "A Novel Method for Synthesizing EuS Nanocrystals From a Single-Source Precursor Under White LED Irradiation" *Chem. Commun.* **2005**, 242-243.

70. Regulacio, M. D.; Tomson, N.; Stoll, S. L. "Dithiocarbamate Precursors for Rare-Earth Sulfides" *Chem. Mater.* **2005**, *17*, 3114–3121.

71. Mourdikoudis, S.; Liz-Marzán, L. M. "Oleylamine in Nanoparticle Synthesis" *Chem. Mater.* **2013**, *25*, 1465–1476.

72. Steckel, J. S.; Yen, B. K. H.; Oertel, D. C.; Bawendi, M. G. "On the Mechanism of Lead Chalcogenide Nanocrystal Formation" *J. Am. Chem. Soc.* **2006**, *128*, 13032–13033.

73. Evans, C. M.; Evans, M. E.; Krauss, T. D. "Mysteries of TOPSe Revealed: Insights Into Quantum Dot Nucleation" *J. Am. Chem. Soc.* **2010**, *132*, 10973–10975.

74. García-Rodríguez, R.; Hendricks, M. P.; Cossairt, B. M.; Liu, H.; Owen, J. S. "Conversion Reactions of Cadmium Chalcogenide Nanocrystal Precursors" *Chem. Mater.* **2013**, *25*, 1233–1249.

75. Sowers, K. L.; Swartz, B.; Krauss, T. D. "Chemical Mechanisms of Semiconductor Nanocrystal Synthesis" *Chem. Mater.* **2013**, *25*, 1351–1362.

76. Evans, W. "Perspectives in Reductive Lanthanide Chemistry" *Coord. Chem. Rev.* **2000**, *206-207*, 263–283.

77. Brown, T.; LeMay, H. E.; Bursten, B.; Murphy, C.; "Chemistry the Central Science", 10th Ed., Pearson-Prentice Hall, 2006, NJ. Appendix E.

78. Hasegawa, Y.; Adachi, T.-A.; Tanaka, A.; Afzaal, M.; O'Brien, P.; Doi, T.; Hinatsu, Y.; Fujita, K.; Tanaka, K.; Kawai, T. "Remarkable Magneto-Optical Properties of Europium Selenide Nanoparticles with Wide Energy Gaps" *J. Am. Chem. Soc.* **2008**, *130*, 5710–5715.

79. Tanaka, A.; Adachi, T.-A.; Hasegawa, Y.; Kawai, T. "Crystal Growth of Nanoscaled Europium Selenide Having Characteristic Crystal Shapes" *J. Alloys Compd.* **2009**, *488*, 538–540.

80. Maneeprakorn, W.; Nguyen, C. Q.; Malik, M. A.; O'Brien, P.; Raftery, J. "Synthesis of the Nickel Selenophosphinates [Ni(Se_2PR_2)$_2$] (R = iPr, tBu and Ph) and Their Use as Single Source Precursors for the Deposition of Nickel Phosphide or Nickel Selenide Nanoparticles" *Dalton Trans.* **2009**, *17*, 2103–2106.

81. Maneeprakorn, W.; Malik, M. A.; O'Brien, P. "The Preparation of Cobalt Phosphide and Cobalt Chalcogenide (CoX, X = S, Se) Nanoparticles From Single Source Precursors" *J. Mater. Chem.* **2010**, *20*, 2329–2335.

82. Panneerselvam, A.; Nguyen, C.; Waters, J.; Malik, M.; O'Brien, P.; Raftery, J.; Helliwell, M. "Ligand Influence on the Formation of P/Se Semiconductor Materials From Metal–Organic Complexes" *Dalton Trans.* **2008**, 4499–4506.

83. Burin, M. E.; Pushkarev, A. P.; Fukin, G. K.; Rumyantsev, R. V.; Konev, A. N.; Bochkarev, M. N. "Synthesis of EuS and EuSe Particles via Thermal Decomposition of Dithio- and Diselenophosphinate Europium Complexes" *Nanotechnol Russia* **2017**, *12*, 66–72.

84. Cossairt, B. M.; Owen, J. S. "CdSe Clusters: at the Interface of Small Molecules and Quantum Dots" *Chem. Mater.* **2011**, *23*, 3114–3119.

85. Pickett, N.; O'Brien, P. "Syntheses of Semiconductor Nanoparticles Using Single-Molecular Precursors" *The Chemical Record* **2001**, *1*, 467–479.

86. Houtepen, A. J.; Koole, R.; Vanmaekelbergh, D.; Meeldijk, J.; Hickey, S. G. "The Hidden Role of Acetate in the PbSe Nanocrystal Synthesis" *J. Am. Chem. Soc.* **2006**, *128*, 6792–6793.

87. Bullen, C. R.; Mulvaney, P. "Nucleation and Growth Kinetics of CdSe Nanocrystals in Octadecene" *Nano Lett.* **2004**, *4*, 2303–2307.

88. van Embden, J.; Mulvaney, P. "Nucleation and Growth of CdSe Nanocrystals in a Binary Ligand System" *Langmuir* **2005**, *21*, 10226–10233.

89. Yu, W. W.; Wang, Y. A.; Peng, X. "Formation and Stability of Size-, Shape-, and Structure-Controlled CdTe Nanocrystals: Ligand Effects on Monomers and Nanocrystals" *Chem. Mater.* **2003**, *15*, 4300–4308.

90. Smith, D. K.; Luther, J. M.; Semonin, O. E.; Nozik, A. J.; Beard, M. C. "Tuning the Synthesis of Ternary Lead Chalcogenide Quantum Dots by Balancing Precursor Reactivity" *ACS Nano* **2011**, *5*, 183–190.

91. Liu, H.; Owen, J. S.; Alivisatos, A. P. "Mechanistic Study of Precursor Evolution in Colloidal Group II−VI Semiconductor Nanocrystal Synthesis" *J. Am. Chem. Soc.* **2007**, *129*, 305–312.

92. Ruberu, T. P. A.; Albright, H. R.; Callis, B.; Ward, B.; Cisneros, J.; Fan, H.-J.; Vela, J. "Molecular Control of the Nanoscale: Effect of Phosphine–Chalcogenide Reactivity on CdS–CdSe Nanocrystal Composition and Morphology" *ACS Nano* **2012**, *6*, 5348–5359.

93. Sung, T. K.; Kang, J. H.; Jang, D. M.; Myung, Y.; Jung, G. B.; Kim, H. S.; Jung, C. S.; Cho, Y. J.; Park, J.; Lee, C.-L. "CdSSe Layer-Sensitized TiO_2 Nanowire Arrays as Efficient Photoelectrodes" *J. Mater. Chem.* **2011**, *21*, 4553–4559.

94. Dai, Q.; Wang, Y.; Li, X.; Zhang, Y.; Pellegrino, D. J.; Zhao, M.; Zou, B.; Seo, J.; Wang, Y.; Yu, W. W. "Size-Dependent Composition and Molar Extinction Coefficient of PbSe Semiconductor Nanocrystals" *ACS Nano* **2009**, *3*, 1518–1524.

95. Morris-Cohen, A. J.; Frederick, M. T.; Lilly, G. D.; McArthur, E. A.; Weiss, E. A. "Organic Surfactant-Controlled Composition of the Surfaces of CdSe Quantum Dots" *J. Phys. Chem. Lett.* **2010**, *1*, 1078–1081.

96. Llanos, J.; Sanchez, V.; Mujica, C.; Buljan, A. "Synthesis, Physical and Optical Properties, and Electronic Structure of the Rare-Earth Oxysulfides Ln_2O_2S (Ln= Sm, Eu)" *Mat. Res. Bull.* **2002**, *37*, 2285–2291.

97. Sarmadian, N.; Saniz, R.; Partoens, B.; Lamoen, D. "Easily Doped P-Type, Low Hole Effective Mass, Transparent Oxides" *Sci. Rep.* **2016**, 1–9.

98. Pinto, A. H.; Leite, E. R.; Longo, E.; de Camargo, E. R. "Crystallization at Room Temperature From Amorphous to Trigonal Selenium as a Byproduct of the Synthesis of Water Dispersible Zinc Selenide" *Mat. Lett.* **2012**, *87*, 62–65.

99. Xie, Q.; Dai, Z.; Huang, W.; Zhang, W.; Ma, D.; Hu, X.; Qian, Y. "Large-Scale Synthesis and Growth Mechanism of Single-Crystal Se Nanobelts" *Crystal Growth & Design* **2006**, *6*, 1514–1517.

100. Zhang, R.; Tian, X.; Ma, L.; Yang, C.; Zhou, Z.; Wang, Y.; Wang, S. "Visible-Light-Responsive T-Se Nanorod Photocatalysts: Synthesis, Properties, and Mechanism" *RSC Adv.* **2015**, *5*, 45165–45171.

101. Jiang, F.; Cai, W.; Tan, G. "Facile Synthesis and Optical Properties of Small Selenium Nanocrystals and Nanorods" *Nanoscale Res. Lett.*, **2017**, *12*, 401–406.

102. Ahn, S.; Jung, S.; Gwak, J.; Cho, A.; Shin, K.; Yoon, K.; Park, D.; Cheong, H.; Yun, J. H. "Determination of Band Gap Energy (Eg) of $Cu_2ZnSnSe_4$ Thin Films: on the Discrepancies of Reported Band Gap Values" *Appl. Phys. Lett.* **2010**, *97*, 021905–1-021905-3.

103. Zhong, X.; Han, M.; Dong, Z.; White, T. J.; Knoll, W. "Composition-Tunable $Zn_xCd_{1-x}Se$ Nanocrystals with High Luminescence and Stability" *J. Am. Chem. Soc.* **2003**, *125*, 8589–8594.

104. Koh, W.-K.; Yoon, Y.; Murray, C. B. "Investigating the Phosphine Chemistry of Se Precursors for the Synthesis of PbSe Nanorods" *Chem. Mater.* **2011**, *23*, 1825–1829.

105. Hendricks, M.; Campos, M.; Cleveland, G.; Jen-La Plante, I.; Owen, J. "A Tunable Library of Substituted Thiourea Precursors to Metal Sulfide Nanocrystals" *Science* **2015**, *348*, 1226–1230.

106. Campos, M. P.; Hendricks, M. P.; Beecher, A. N.; Walravens, W.; Swain, R. A.; Cleveland, G. T.; Hens, Z.; Sfeir, M. Y.; Owen, J. S. "A Library of Selenourea Precursors to PbSe Nanocrystals with Size Distributions Near the Homogeneous Limit" *J. Am. Chem. Soc.* **2017**, *139*, 2296–2305.

107. Owen, J. S.; Chan, E. M.; Liu, H.; Alivisatos, A. P. "Precursor Conversion Kinetics and the Nucleation of Cadmium Selenide Nanocrystals" *J. Am. Chem. Soc.* **2010**, *132*, 18206–18213.

108. Wang, F.; Richards, V. N.; Shields, S. P.; Buhro, W. E. "Kinetics and Mechanisms of Aggregative Nanocrystal Growth" *Chem. Mater.* **2013**, *26*, 5–21.